The Basics of Orbital Imaging

David Ornan and Joseph Donahue

Introduction

While many pathologic processes intrinsic to the globe may be easily evaluated under direct visualization, the ophthalmologist is more reliant upon imaging for the evaluation of orbital and intracranial processes that may affect a patient's vision. In the olden days of radiology when ophthalmologists' options were limited to conventional radiography, only advanced disease secondarily affecting osseous structures or producing calcification would have been visible, and even then, probably only subtly. In current practice, orbital radiography has been nearly completely abandoned and is now only utilized for the detection of metallic foreign bodies that might preclude MRI, and in rare instances, when CT is unavailable and there is suspicion for gross fracture.

Beginning with computed tomography (CT) in the early 1970s and later magnetic resonance imaging (MRI) in the 1980s, cross-sectional imaging became the primary tool for evaluation of orbital and intracranial pathology. These technologies were applied to vascular imaging in the form of CTA and MRA, and additional advances were made in conventional angiography with the advent of digital subtraction angiography (DSA), CT arteriography, and various interventional techniques. These modalities are constantly evolving, and it is important for ophthalmologists to be aware of all the options in their imaging armamentarium so that they may order the safest, most appropriate study. This chapter will focus on basic imaging physics, indications, and contraindications of routine and more advanced CT, MR, and angiographic techniques, as well as briefly cover some image-guided orbital interventions.

D. Ornan, M.D. (✉) • J. Donahue, M.D.
Department of Radiology, University of Virginia Medical Center, 1215 Lee Street, PO Box 800170, Charlottesville, VA 22908-0170, USA
e-mail: dao2a@virginia.edu; JD2UC@hscmail.mcc.virginia.edu

Computed Tomography

Physics/Basics

CT imaging is based on the differential absorption of X-rays by tissues of varying density within the body. A CT scanner consists of a rotating ring, with an X-ray source on one end and an array of detectors on the opposite end. The detectors measure the amount of radiation transmitted through a given axial slice of the body. The data is analyzed by a computer and each point, or picture element (pixel), within the slice is assigned a numerical density value based on how much radiation passes through it. A two-dimensional density map is subsequently generated. To display the density map as a black and white picture, the numerical density value of each pixel is presented on a scale of units known as Hounsfield units (HU), in which the density of water is arbitrarily assigned a value of 0. The higher the number, the brighter the pixel appears on the image, and vice versa. Hounsfield units range from +1,000 (metal) to −1,000 (air). In CT parlance, structures are described as isodense, hyperdense, or hypodense, with skeletal muscle often used as the standard mid-range density structure. The terms "level" and "window width" describe the way in which individual pixels are displayed on a gray-scale image based on their HU. The level is the HU value which is assigned the most intermediate gray color. The window width is the numerical range of HU between black and white. Since the human eye can only distinguish about 16 different shades of gray, the window width is divided by 16 to determine the HU values which are included in each individual gray tone. For example, if the level is set at 0, water will be assigned the most intermediate gray color. If the width is 1,600, each gray tone will cover a range of 100 HU. If the range is very wide, in order for two adjacent structures to be distinguished, they must be very different in density. Hence, subtle differences in density are best visualized with a narrower window width. PACS systems have preset window width and level settings (e.g., soft

tissue windows, lung windows, bone windows); however, they can be manually changed according to user preference. An appropriate setting for evaluation of orbital structures would be a window width of 350–400 HU and a level of 80–100 HU. Osseous structures would be better evaluated with a window wider than 1,000 HU. In contradistinction to window/level settings which can be actively manipulated on the PACS station, algorithms are preprogrammed software filters applied during the reconstruction of the primary data set which artificially accentuates either soft tissue or osseous structures. Both soft tissue and bone algorithms are automatically sent to PACS and each should be reviewed separately as part of a routine search pattern. In many cases, subtle osseous findings such as hairline fractures or tumoral calcification can be missed if the interpreter views only the soft tissue algorithm images using bone windows. Conversely, subtle differences in soft tissue density can be missed if the bone algorithm images are evaluated in soft tissue windows (for example, the presence of fluid density within a tumor to suggest internal necrosis).

First generation scanners only generated images one slice at a time, with the patient moved manually for each rotation of the X-ray tube [1]. Later generation scanners with faster processors allowed for the patient to be continuously passed through the gantry as it rotated, producing a helically acquired data set [2]. On older scanners, orbital CT images would first be obtained in the axial plane. The technician would then tilt the entire gantry so that direct coronal acquisitions could be obtained, irradiating the patient a second time. The newest CT scanners now have multiple X-ray detectors which allow for the acquisition of multiple slices through the body with each rotation of the gantry. This allows for extremely rapid acquisition of very thin sections through the orbits, which can then be reconstructed in exquisite detail in any plane desired. Cutting edge 320-slice scanners are now capable of generating 0.5 mm images over a 160 mm scan width for every rotation of the gantry. Ding et al. have shown that CT angiographic depiction of the tiny anterior ethmoidal artery using this technology is similar in accuracy to that of digital subtraction angiography, the current gold standard [3].

Although CT and MR play complimentary roles in many ophthalmologic cases, CT possesses many advantages that often make it the initial imaging test wielded by clinicians (Table 9.1) [4]. Primary among these is simply the ease with which it can be obtained. Whereas many institutions do not yet offer 24 h MR coverage, CT scanners are ubiquitous in emergency departments. They offer a great deal of clinically relevant information in a very short period of time and at a relatively low cost. Figure 9.1 demonstrates some normal anatomic structures in axial, coronal, and sagittal planes. For

Table 9.1 Commonly encountered absorption values in orbital CT

Hounsfield unit	Fluid or tissue
−1,000	Air
−70 to −100	Fat
0	Water
4–10	Cerebrospinal fluid
35–45	Brain
−1,000	Bone

the ophthalmologist and neurologist, it acts as a very effective screening tool that can detect actionable emergent pathology which can then be followed with MR as clinically warranted. Aside from these considerations, CT is the test of choice when high spatial resolution is desired and when there is suspicion for hemorrhage, mineralization, and/or osseous involvement. MR, on the other hand, is notable for its exquisite soft tissue contrast resolution, which of course lends itself to evaluation of anatomically complex soft tissue structures such as the brain and cranial nerves. CT is usually sufficient in cases of orbital trauma for evaluation of subtle fractures, optic nerve avulsion, or the presence of foreign bodies (Fig. 9.2). Additionally, it can easily depict infectious or inflammatory processes in the setting of acute proptosis and at least localize, if not fully characterize, a mass lesion in the setting of papilledema or bitemporal hemianopsia (for example, pituitary apoplexy). It plays a complimentary role in the evaluation of calcified tumors such as retinoblastoma and craniopharyngioma and both primary and secondary bone lesions such as fibrous dysplasia, metastases, and hyperostosis adjacent to a meningioma. Box 9.1 and Table 9.2 summarize the indications for CT and MRI. In some situations, CT must suffice when MR would otherwise be the preferable modality but is contraindicated due to implantable electronic devices, severe claustrophobia, ferromagnetic foreign bodies, and obesity.

As a general rule, iodinated contrast material improves the conspicuity of nontraumatic orbital and periorbital lesions. In the setting of suspected inflammation, infection, or neoplasm, contrast should always be administered, except in cases in which there are obvious contraindications, such as acute renal failure or history of severe allergic reaction (Fig. 9.3). The risk of contrast-induced renal failure is increased in patients with borderline renal function, diabetes, multiple myeloma, and dehydration. In the setting of acute trauma, contrast could potentially act as a confounding factor since it would be indistinguishable from hyperdense hemorrhage. Additionally, contrast material would be contraindicated in the evaluation of thyroid ophthalmopathy, since it could potentially exacerbate systemic thyroid disease and interfere with eventual radioactive iodine therapy [5, 6].

Fig. 9.1 Contrast-enhanced orbital CT in soft tissue windows: normal anatomy. (**A**) Axial image demonstrates right optic nerve (*asterisk*), left lens (*yellow arrow*), and paper thin lamina papyracea (*blue arrow*). (**B**) Coronal reconstruction demonstrates right superior ophthalmic vein (*yellow arrow*). The extraocular musculature is best evaluated in this plane (*blue arrow*). (**C**) Sagittal reconstruction demonstrates optic canal (*yellow arrow*)
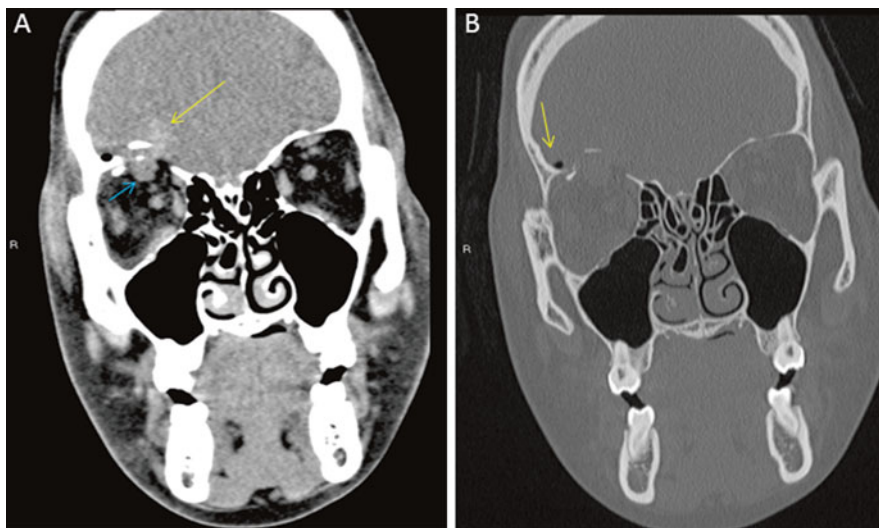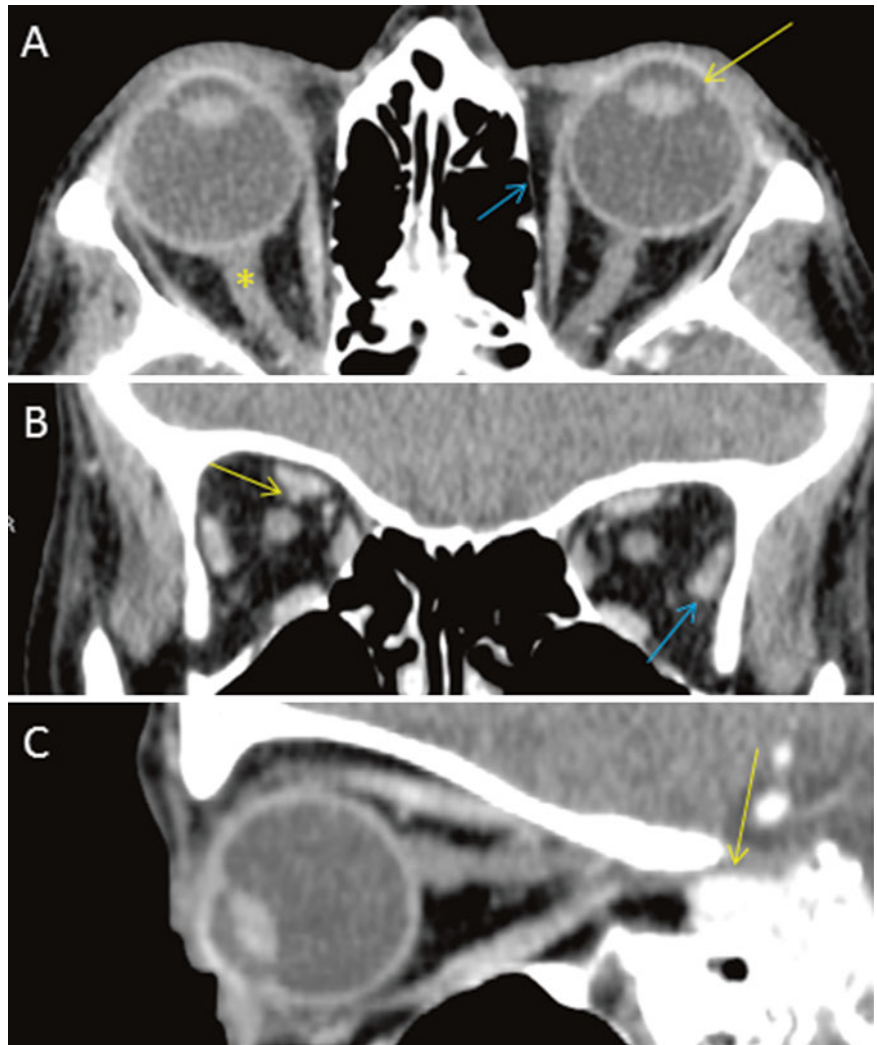
Fig. 9.2 A disagreement "taken outside": stiletto to the eye. (**A**) Coronal non-contrast CT in soft tissue windows demonstrates intracranial hemorrhage (*yellow arrow*) associated with orbital roof fracture. There is asymmetric reticulation of the intraconal fat on the right and enlargement of the superior rectus muscle (*blue arrow*), suggesting contusion. (**B**) Bone windows better demonstrate comminuted fracture margins as well as focus of pneumocephalus (*yellow arrow*). Note that the hemorrhage is invisible on bone windows

CTA

As opposed to routine post-contrast CT scans which generally acquire images in the venous phase, CTA involves the rapid acquisition of images earlier after injection, when contrast still opacifies the arterial system. As mentioned, advances in technology now enable characterization of arteries previously only visible on conventional angiograms. Ophthalmologic indications for CTA include evaluation for

---

Box 9.1 CT Imaging Parameters for Orbits
High resolution orbits
0.63 mm axials
Pitch 1
Table speed 1.25 cm/s
Intravenous contrast medium
Field of view 13 cm

**Table 9.2** Advantages and disadvantages of CT and MRI

	Advantages	Disadvantages
CT	Availability and fast examination time	Ionizing radiation
	Evaluation of bony involvement	Contrast reaction
		Beam-hardening and other artifacts
MRI	Detects virtually all lesions of the orbit except trauma	Motion and other artifacts
	No ionizing radiation	Missile and thermal injuries
		Incompatible with a number of medical devices and metal implants
		Longer scanning times
		Overweight and claustrophobic patients cannot be accommodated

aneurysmal causes of cranial neuropathy, amaurosis fugax, atherosclerotic stenosis, dissection, vasospasm, arteriovenous malformations, and carotid-cavernous fistulas. The advantages of CTA over MRA include rapid image acquisition, more accurate depiction of stenosis, and spatial resolution. For example, a small proximally tortuous branch vessel could mimic an aneurysm on MRA, but would be easily delineated on CTA. CT venography, in contrast, acquires images in the venous phase. Indications for CTV include suspected venous sinus thrombosis in the setting of proptosis, papilledema, or cranial nerve palsy.

Routine Imaging Protocol

At our institution, the standard orbital CT protocol calls for the acquisition of 0.625 mm axial source images which are then reconstructed as overlapping 1.25 mm slices and sent to PACS in both soft tissue and bone algorithms. Additionally, overlapping 1.5 mm sagittal and coronal reformatted images are also routinely generated by the technicians (Box 9.2). The source 0.625 mm source data set may also be sent to PACS for problem solving as necessary, which can then be manipulated in real-time into any plane desired. Curved reformatted images can also be employed to better depict curvilinear structures in a single plane. The decision to administer intravenous contrast is left to the clinician with guidance provided by the radiologist as necessary.

Aside from the relatively limited soft tissue contrast resolution, the major disadvantage of CT is radiation exposure, particularly in younger patients [7]. Unfortunately, the lens is one of the most radiosensitive structures in the human body. For neuroimaging purposes, commonly used 16-slice CT scanners deliver a lens dose ranging from 80 to 100 mGy [8]. Recently, the International Commission on Radiological
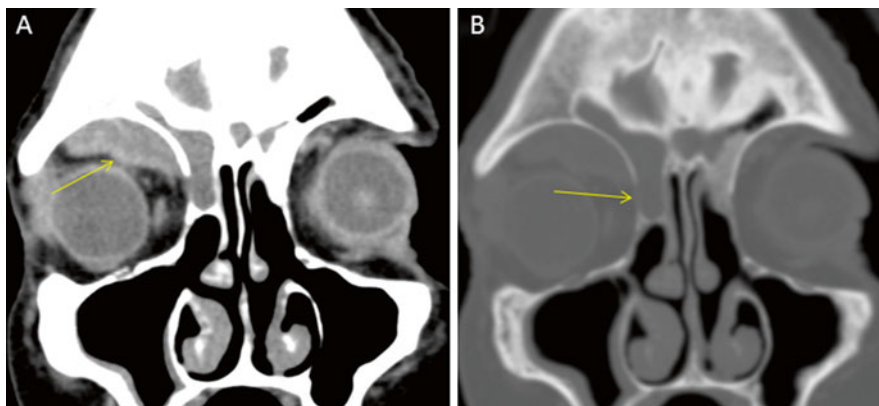
Fig. 9.3 Subperiosteal abscess originating from frontoethmoidal sinusitis. (**A**) Contrast-enhanced coronal CT in soft tissue windows demonstrates peripherally enhancing subperiosteal abscess (*arrow*) on the right, displacing the superior rectus muscle and globe inferiorly. The right frontal sinus is completely opacified indicating extensive mucosal inflammatory disease. (**B**) Coronal CT in bone windows demonstrates focal defect (*arrow*) in the lamina papyracea through which the infection spread

Protection (ICRP) significantly lowered the putative human threshold value for cataractogenesis to 0.5 Gy (acute or cumulative prolonged exposure) from 2 Gy [9]. In addition

to automatic tube current modulation, newer techniques such as adaptive statistical iterative reconstruction (ASIR) algorithms have been applied with some success to lower dose while maintaining adequate image quality, but they are not fully optimized [10]. The long-term cancer risk remains controversial; however, it is an important consideration to bear in mind when ordering diagnostic studies.

Box 9.2 Indications for CT and MRI	
CT	MRI
Orbitocranial trauma	Detection of orbital masses
Orbitocranial hemorrhage	Evaluation of orbital and ocular masses
Detection of orbital masses	Evaluation of sinuses
Evaluation of orbital bones	Evaluation of optic pathway
Evaluation of sinuses	Orbital changes secondary to ocular tumors
Detection of calcification	Orbitocranial hemorrhage

Artifacts

As with any imaging modality, CT can produce artifacts which can limit the diagnostic quality of a study (Fig. 9.4). Artifacts that are unique to CT include beam hardening artifact and detector artifact. Beam hardening artifact is caused by high density structures which "harden" the transiting X-ray beam by absorbing the lower energy photons and allowing only higher energy photons to pass through.
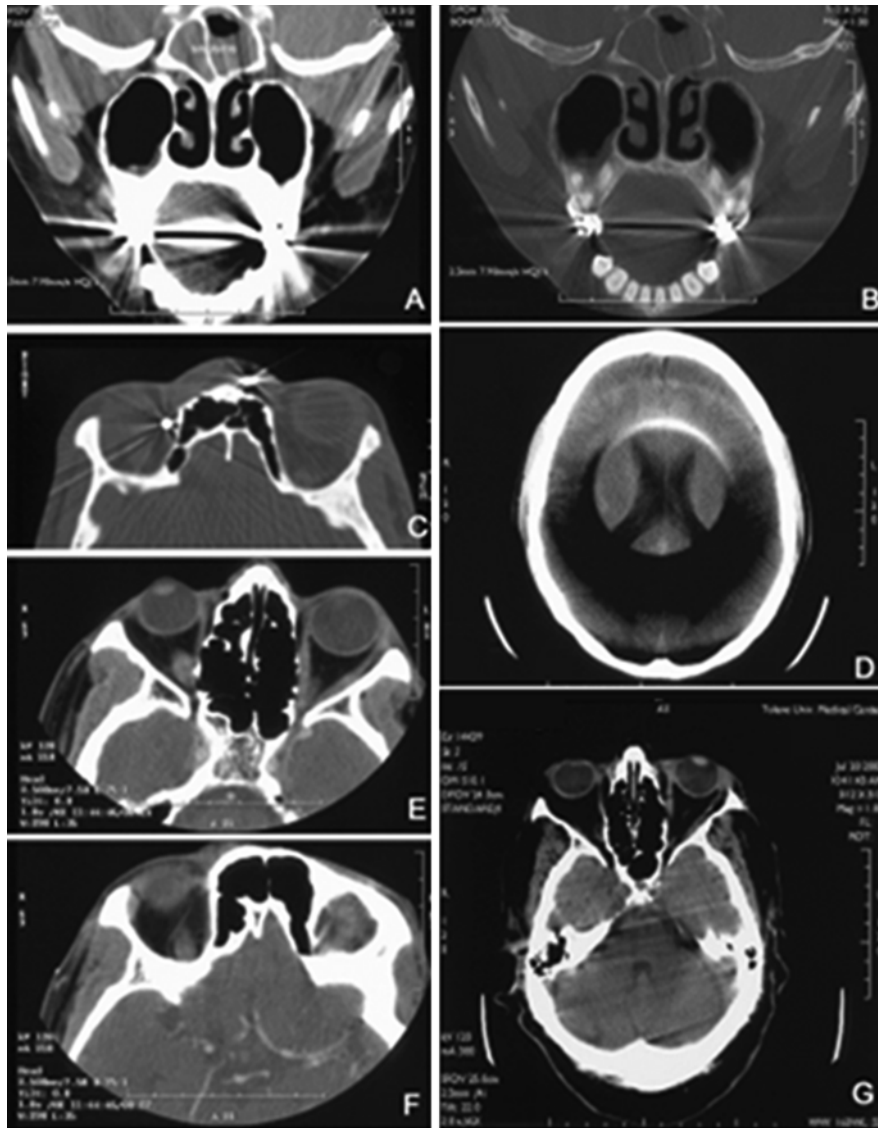
Fig. 9.4 CT Artifacts. (**A**) Dental fillings causing streak artifacts. (**B**) Artifact in the patient shown in (**A**) is reduced in bone windows. (**C**): Shotgun pellets causing streak artifacts. (**D**) Detector ring artifact. (**E**, **F**) Positioning artifacts. (**G**) Distortion due to patient motion

This can create dark bands between osseous structures and in particular often degrades images through the posterior fossa and at the orbital apex. Beam hardening also contributes to metallic streak artifact, which can sometimes render a CT scan nondiagnostic. Common causes of metallic streak artifact include dental amalgams and orbital foreign bodies. Faulty detectors can produce circular or ring-shaped artifacts. Other artifacts such as partial volume averaging and motion artifact can plague any cross-sectional modality. Partial volume averaging occurs when the interface of two adjacent tissues of different density is indistinct because of the computer's need to compress a three-dimensional space into a two-dimensional image. The interface is depicted as an average of the two densities, which can create the illusion of a lesion.

Table 9.3 Commonly encountered signal types in orbital MRI

	Signal type		
Tissue type	Tl-weighted	T2-weighted	Fat suppression
Globe	Hypo (dark gray)	Hyper (white)	Hypo (dark gray)
Fat	Hyper (white)	Hypo (white)	Intermediate (gray)
Extraocular muscle	Hypo (dark gray)	Hypo (light gray)	Hyper (white)
Optic nerve	Hyper (light gray)	Hypo (light gray)	Hyper (light gray)
Cerebrospinal fluid	Hyper (dark gray)	Hyper (white)	Hypo (dark gray)
Bone	Void (black)	Void (black)	Void (black)
Vessels	Void (black)	Void (black)	Void (black)

Magnetic Resonance Imaging

Physics/Basics

The basis of all MR imaging is the behavior of protons in an external magnetic field. The reason that protons are susceptible to an external magnetic field is simply that protons themselves are tiny magnets. The proton nucleus spins like a top, and as it spins the positive nuclear charge rotates as well. The rotating charge of the nucleus creates a small current, and the small current induces a small magnetic field. In a strong and uniform external magnetic field, the magnetic fields of the spinning protons align with the external magnetic field [11]. The sum of the proton magnets aligned parallel to the external field is greater than those aligned antiparallel, and thus creates a net vector in the longitudinal direction (basis of T1-weighted images). The protons also behave like a spinning top in that they wobble, or precess, as they spin and produce a magnetic vector transverse to the external magnetic field (basis of T2-weighted images).

A radiofrequency pulse (RF pulse) perturbs the proton vectors such that some protons flip into the high-energy anti-parallel orientation; this decreases the vector sum in the longitudinal (T1) direction. Simultaneously, the RF pulse synchronizes the proton wobble creating a greater transverse vector (T2). The recovery of the longitudinal (T1) vector, and thus T1 signal strength, is achieved when the high-energy anti-parallel protons relax back to the lower-energy parallel orientation. The speed at which this occurs, or relaxation time, is influenced by how quickly the energy released during the flip can be absorbed by the surrounding tissues. Fat facilitates the flip and is therefore hyperintense, while water delays the T1 relaxation, and is thus dark or hypointense.

Protons within water-rich tissues are abundant and freely mobile. They therefore maintain the T2 transverse vector strength longer, such that the T2 signal of aqueous humor or CSF, for instance, is bright. In contrast, protons bound to macromolecules in membranes such as the choroid are less abundant and less mobile, and therefore quickly lose T2 transverse vector strength as the proton wobble desynchronizes and are displayed as dark or hypointense on T2-weighted images [12, 13].

Routine Imaging Protocol

Specific sequences and corresponding appearance of selected structures are detailed in Table 9.3. Generally speaking, most pathology demonstrates high T2 signal, and T1-weighted images provide the best overall anatomic detail (Fig. 9.5). Several important substances demonstrate high T1 signal: fat, subacute blood, and often melanin (choroidal melanoma). T2 and FLAIR sequences are indispensable in the evaluation of demyelinating disorders, in which demyelinating foci are conspicuously T2 hyperintense. Some specialized highly T2-weighted sequences, such as CISS, provide excellent resolution of the cranial nerve courses through the basilar cisterns. Diffusion Weighted Images (DWI) and the Apparent Diffusion Coefficient (ADC) are key in evaluating acute ischemia, as may be suspected in acute post-chiasmal vision loss [14].

Post-contrast images are generally performed using T1-weighted sequences with fat saturation technique, meaning the fat signal is selectively suppressed such that contrast enhancement is accentuated. Pre-contrast T1 images are generally not performed with fat saturation as most orbital pathology typically demonstrates T1 hypointensity, and fat saturation would diminish the contrast between the lesion and the surrounding orbital fat (Figs. 9.6 and 9.7) [12].

MRI is most commonly performed with 1.5 or 3 T units using either head or surface coils. Surface coils are applied directly to the head and receive the signal emitted by the tissue.
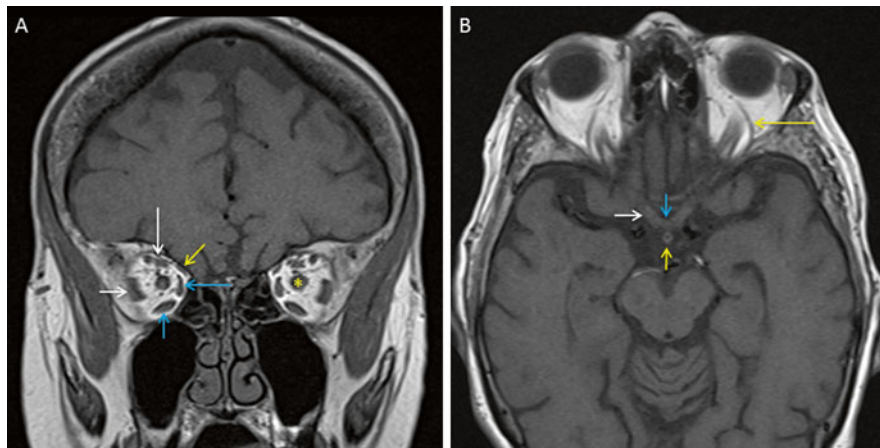
Fig. 9.5 Orbital MRI: normal anatomy. (**A**) Coronal T1 pre-contrast. Extra-ocular musculature: Lateral rectus (*short white arrow*), superior rectus (*long white arrow*), medial rectus (*long blue arrow*), inferior rectus (*short blue arrow*), superior oblique (*yellow arrow*). optic nerve (*asterisk*). (**B**) Axial T1 pre-contrast. Optic nerve (*short white arrow*), optic chiasm (*blue arrow*), pituitary stalk (*short yellow arrow*), superior ophthalmic vein (*long yellow arrow*)
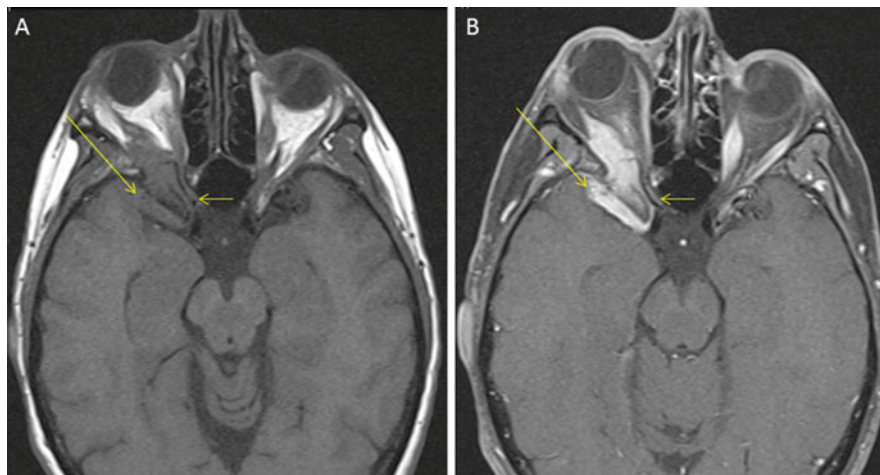
Fig. 9.6 Sphenoid wing meningioma with orbital extension. T1 pre-contrast (**A**) and T1 post-contrast fat-suppressed sequences (**B**). Meningioma involving the greater wing of the right sphenoid bone (*long arrows*) with orbital extension and resultant proptosis. Compromises of the orbital apex (*short arrows*) are well demonstrated with MRI. Note that post-contrast images are identifiable by nasal mucosal contrast enhancement. Fat suppression helps delineate enhancing tumor from the intrinsically T1 hyperintense orbital fat

The increased signal-to-noise ratio that surface coils provide translates to higher spatial resolution. However, surface coil signal quickly deteriorates within the posterior orbit, so practically surface coil imaging is reserved for disorders of the orbit anterior to the apex [15].

MRA

Magnetic resonance angiography may be added to conventional MRI protocols when interrogation of the major intracranial vessels is necessary, for instance in the case of suspected 3rd nerve palsy, cavernous carotid fistula, arterial dissection, or vascular malformation. MRA may be performed using either of two techniques, Time of Flight (TOF) or Phase contrast (PC). TOF is generally considered the more robust technique and may be performed alone or with the addition of gadolinium-based intravenous contrast medium [16].

Although the spatial resolution of MRA is less than that of CTA, MRA is generally capable of resolving vascular causes of ophthalmologic symptoms with two caveats: MRA sensitivity for small aneurysms (<3 mm) is somewhat limited; MRA tends to overestimate the degree of arterial stenosis. As with other MR applications, MRA is more susceptible to motion artifact than CTA. Gadolinium is less nephrotoxic
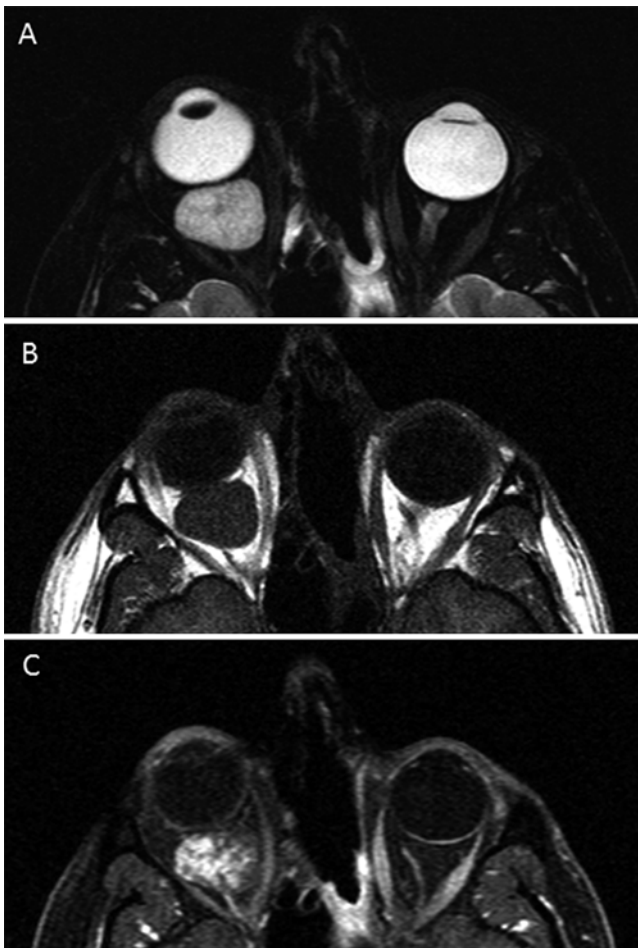
Fig. 9.7 Orbital hemangioma. (**A**): Axial fat-suppressed turbo spin echo T2 sequence demonstrates T2 hyperintense mass in the right intraconal space with resultant proptosis. (**B**): Axial non-contrast T1 spin echo T1 sequence demonstrates corresponding T1 hypointense signal. (**C**) Post-contrast fat-supressed spin echo T1 sequence demonstrates heterogeneous enhancement. Notice the importance of fat suppression in helping to distinguish enhancement from normal surrounding orbital fat

importance of scrutinizing the source images of the TOF angiogram, as well as the pre-contrast T1-weighted images to evaluate for intrinsically T1 hyperintense structures adjacent to or within the major intracranial arteries [16].

MRV

In patients with symptoms such as papilledema and cranial nerve palsies, or for whom there is other specific concern for dural venous sinus thrombosis, MRI offers strong venography capabilities. MR venography may be performed with variations on the same techniques as MRA, PC, TOF, and contrast-enhanced venography. Common pitfalls of non-contrast MR venography are related to asymmetric flow, as seen in sinus hypoplasia with resultant slow flow which may be mistaken as thrombosis. As seen in TOF MRA, the MR signal characteristics of thrombosis in various stages of acuity may simulate a patent sinus. Contrast-enhanced MRV, similar in principle to CTV, fills the dural venous sinuses with contrast agent, and thus is less susceptible to the aforementioned pitfalls.

Perfusion

Perfusion-weighted imaging (PWI) is a contrast-enhanced technique for quantifying the volume and rate of parenchymal perfusion at the capillary level. At present the technique does not have any widely accepted application specifically within the orbit. However, in the setting of acute post-chiasmatic CVA-related visual deficits, PWI may be paired with DWI to distinguish penumbra (at risk, but not yet irreversibly infarcted tissue) from an ischemic infarct core (restricted diffusion). The presence and volume of penumbra may inform decisions regarding the choice for intervention and preferred thrombolysis method [11].

A non-contrast-enhanced perfusion technique, Arterial Spin-labeled (ASL), is showing promise as a quantitative method of evaluating the perfusion of smaller vascular beds, such as retina and choroid. Although the spatial resolution needed for clinical orbital applications is currently lacking, in the future this technique may provide quantitative perfusion data for the entire volume of the eye [13]. Additionally, the fact that this technique does not require use of intravenous gadolinium agent has benefits beyond circumventing the related contraindications. Multiple scans could be obtained serially in a single session to monitor progress of revascularization or other therapeutic responses because the interstitial tissues and capillary beds have not been contaminated by an intravenous contrast agent [18].

than the iodinated contrast agents necessary for CTA and may be administered when the GFR is above 30 mL/min/1.73 m^2 vs. 45 mL/min/1.73 m^2 for iodinated contrast agents [17].

Caution must be exercised when evaluating TOF MRA. This technique displays blood flow as hyperintense, based on T1 properties, and is susceptible to artifact from other materials with bright T1 characteristics. Fluids with high protein content, such as inspisated sinus secretions within the sphenoid sinus, may simulate aneurysms of the intracranial internal carotid artery. T1 hyperintense methemoglobin within subacute mural thrombi may simulate normal flow and result in false negative evaluation for arterial dissection or sinus thrombosis [12]. These examples emphasize the

Functional Imaging Methods of Orbit

Positron Emission Tomography

Positron emission tomography (PET) generates images based on the decay of intravenously administered 18F-fluoro-2-deoxyglucose (FDG). Measuring the accumulation of FDG, a glucose analog, within tissues, provides functional/metabolic data, which may be co-localized to CT, or less commonly MRI, for more precise anatomic detail. PET/CT is useful in distinguishing radiation necrosis from local tumor progression, dementia etiology, and localizing epileptogenic foci. PET/CT may elucidate functional causes of cortical blindness that are occult to structural imaging, such as occipital hypometabolic foci related to carbon monoxide or cyclosporine toxicity. However, with specific regard to the orbit, PET/CT is basically limited to an adjunct for neoplasm evaluation (namely lymphoma) [19]. The technique is limited by relatively poor spatial resolution (5 mm), cost, and availability of FDG as limited by proximity to producing cyclotron. Additionally, there may be errors in registration of the PET data with CT or MRI images such that structures may erroneously appear as hypermetabolic.

Functional MRI

Functional MRI (fMRI) broadly refers to a variety of MR techniques where real time regional brain activity is detected. This is most typically performed with a blood-oxygen-level-dependent (BOLD) T2-based technique that infers parenchymal activity by measuring regional oxygen consumption. Current clinical applications of fMRI principally relate to delineating regions of functional cortex adjacent to neoplasms and mapping pathways of higher neuronal integration. Although no commercially available applications for fMRI relate specifically to the orbit, research demonstrating task-specific regional retinal fMRI activation mapping has been reported in animal models using higher field strength magnets [20].

Artifacts

MRI is subject to a number of artifacts related both to factors distorting the local magnetic field homogeneity and related to patient motion (Table 9.4) (Fig. 9.8). Currently, there are no MRI sequences available that can totally eliminate motion artifact. The ghosting artifact associated with involuntary globe movements may be reduced by altering several sequencing parameters: orienting the phase encoding direction from left to right rather than anterior to posterior, keeping scan time as short as possible for the patient, and averaging together several of the same sequences to strengthen the signal-to-noise ratios [21]. A technique applied to sequence acquisition may reduce the motion artifact associated with blinking. The Blinking Artifact Reduction Pulse (BARP) allows for the scan to be performed

Table 9.4   MRI artifacts

Artifact	Cause
Wrap around	Wrong field of view
Bioinhomogeneity	Magnetic field distortion by metal objects
Motion	Patient motion during procedure
Flow or pulsation	Misregistration with resulting artifacts
Chemical shift	Usually related to fat protons' resonating at a frequency different from water protons
Partial volume	Related to two different tissues being measured in a single voxel, the resultant display is an average of the two tissues

with the eyes open and fixed to a point, while the BARP corrects for motion occurrences during blinking [22].

Other artifacts relate to local inhomogeneity in the magnetic field during pulse sequence acquisition. Many cosmetics, such as some mascara, contain ferromagnetic pigments with iron oxide bases which can significantly deteriorate signal, often obscuring much of the globe and anterior orbit [23]. Local magnetic field strengths are also slightly different within tissues of varying composition, such that the magnetic field strength within the pneumatized sinuses is slightly greater than within the adjacent orbital fat. This may often result in signal drop out or incomplete fat saturation, classically within the medial orbital apex. Similarly, these local magnetic inhomogenieties caused by distinct but closely apposed tissues may result in spatial misrepresentation of structures within the final computed image, as may be seen with silicone vitreous implant edge artifacts [21].

Conventional Angiography, CT Arteriography, and Interventions

Although most ophthalmologic pathology is better depicted using cross-sectional imaging, conventional angiography continues to play an important role in the diagnosis of several vascular processes. Digital subtraction angiography (DSA) remains the gold standard in diagnosis and characterization of aneurysms due to its superlative spatial resolution. Other major indications for diagnostic orbital angiography include vascular malformations such as AVM and cavernous-carotid fistulas. With the advent of orbital interventional procedures, many diseases can be diagnosed and treated in the same session. Before any intervention is attempted, it is crucial that the angiographer carefully establish the vascular supply of the lesion being treated, including contributions from both the internal carotid and external carotid arteries. This will help guide strategy and avoid complications such as inadvertent embolization of normal structures due to dangerous branch points and anastomoses. In cases of neoplastic involvement of the orbits, the diagnosis is often already established and angiography is performed for treatment

Fig. 9.8 MR artifacts. (**A**) Wrap-around artifact due to wrong field of view. (**B**) Distortion due to iron pigment in patient's mascara. (**C**) Surgical clip results in distortion or shielding of magnetic field. (**D**) Metal artifact due to dental hardware. (**E**) Ghosting from orbital motion. (**F**) Distortion due to head motion

planning purposes. In recent years, CT arteriography has been increasingly employed for investigation of orbital pathology. As mentioned, CTA involves the acquisition of images in the arterial phase after peripheral venous injection of contrast. This inevitably leads to at least some degree of venous contamination and potential obscuration of very fine arterial anatomy. In CT arteriography, multidetector CT is combined with DSA in the same suite so that images can be acquired after direct injection of a selectively catheterized artery using a very small amount of contrast. Hasegawa et al. demonstrated that CT arteriography better characterized the arterial feeders and enhancement pattern of various orbital masses as compared to dynamically enhanced MRI [24].

In general terms, the goal of orbital intervention is to either recanalize an occluded normal vessel or occlude pathological vessels. The normal vessel of major importance that can become occluded in the orbit is the central retinal artery, usually due to thromboembolism. Local intra-arterial fibrinolysis (LIF) involves the injection of thrombolytic agent through a super-selectively catheterized

ophthalmic artery. In 2010, the multicenter randomized EAGLE (European Assessment Group for Lysis in the Eye) trial demonstrated that there was no significant difference in clinical outcome between LIF and conservative treatment in terms of visual improvement. In fact, because of higher complication rates in the LIF cohort, the study was stopped after the first interim analysis [25]. However, efficacy remains controversial, and it remains to be seen whether more stringent selection criteria could produce different results.

Occlusive procedures can be further divided into those that are definitively curative and those that are adjunctive to surgery. Both cavernous-carotid (CC) fistulas and aneurysms can be cured using minimally invasive image-guided techniques. CC fistulas are the result of abnormal, usually post-traumatic shunting of arterial blood into the cavernous sinus through a tear in the cavernous internal carotid artery (Fig. 9.9). Classic symptoms include proptosis, chemosis, cranial nerve palsies, and impaired vision, and the classic angiographic finding is early opacification of the cavernous

Fig. 9.9 Cavernous-carotid fistula. (**A**) Axial CTA demonstrates tear in the right cavernous segment internal carotid artery with contrast emptying into the cavernous sinus (*arrow*). This patient sustained severe head trauma, as evidenced by extensive hyperdense air-hemorrhage levels throughout the ethmoid air cells and sphenoid sinuses. Associated fractures are poorly visualized on these soft tissue algorithm images. (**B**) A more cephalad slice demonstrates classic asymmetric enlargement of the right superior ophthalmic vein (*arrow*)
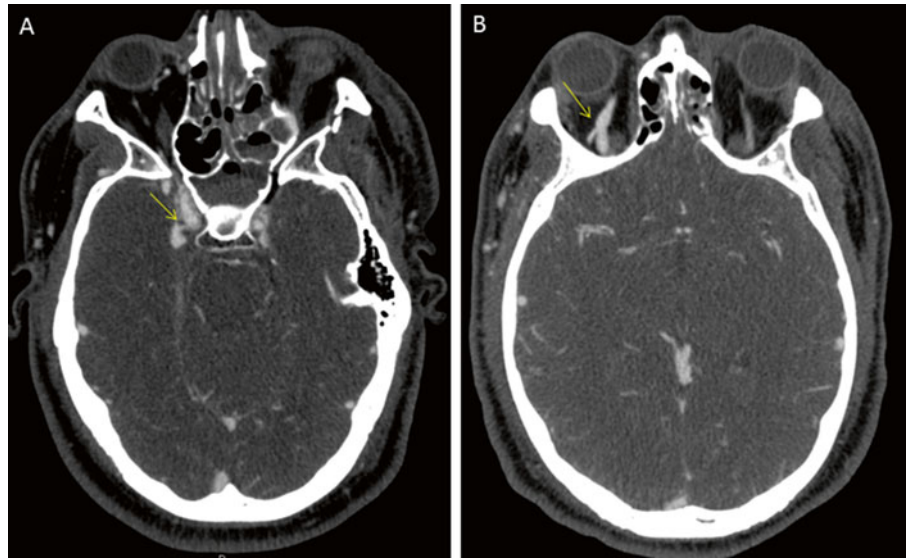

Fig. 9.10 Cavernous-carotid fistula. Lateral projection digital subtraction angiography after ICA injection demonstrates abnormal early opacification of the superior ophthalmic vein (*short arrow*) and pterygoid plexus (*long arrow*)

sinus and superior ophthalmic vein after injection of contrast (Fig. 9.10). In many cases, closure of the fistula can be achieved using either coils or detachable balloons with

preservation of ICA patency (Fig. 9.11). The adjunctive occlusive procedures mainly involve the preoperative embolization of hypervascular orbital or periorbital tumors, including meningiomas (Fig. 9.12), squamous cell carcinomas, metastases, and juvenile nasopharyngeal angiofibromas. The goal is to temporarily occlude feeding vessels using either glue or embolic particles to aid in subsequent excision by the surgeon (Fig. 9.13). In some cases, the goal of embolization is simply palliation in the setting of incurable tumor burden.

One interventional technique that has generated a great deal of interest recently as a potential additional curative measure is intra-arterial chemotherapy for retinoblastoma. Although first described in 1954 through a carotid approach [26], advancements in catheterization techniques have enabled direct injection of chemotherapy into the ophthalmic artery. The chemotherapeutic agent melphalan has been found to be the most effective drug against retinoblastoma; however, it is too toxic to be used systemically. With the intra-arterial approach, very high local doses of drug can be administered with relatively few side effects and very high rates of response and globe salvage [27–29]. This highly effective technique illustrates the recent advances made in the field of interventional neuroradiology and the need for a multidisciplinary approach to treat various orbital pathologies effectively.
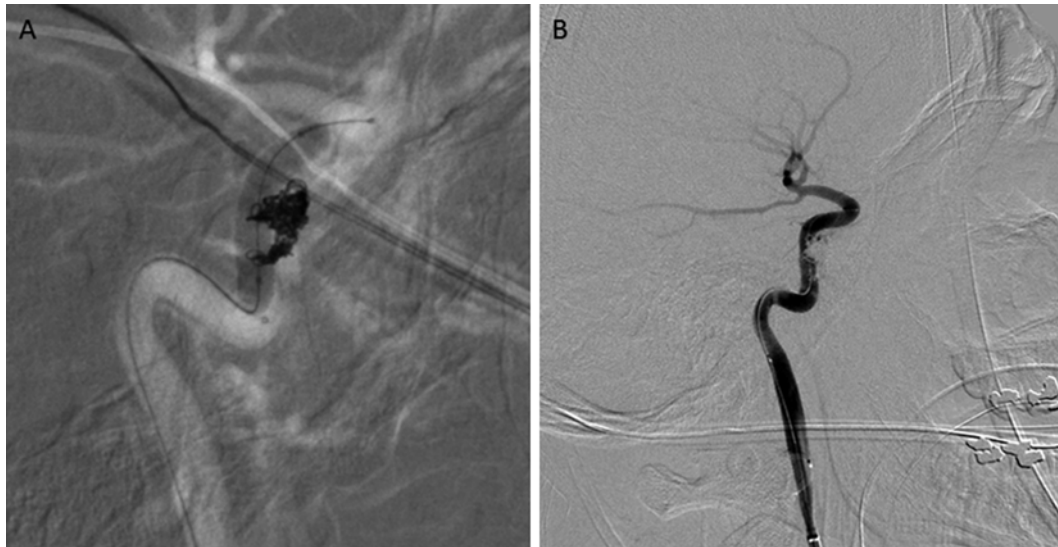
Fig. 9.11 CC fistula repair. (**A**) Lateral projection DSA demonstrates microcatheter in the ICA and multiple coils within the surrounding cavernous sinus. (**B**) Final run angiogram demonstrates patency of the ICA and successful embolization of the fistulous connection as evidenced by lack of early opacification of venous structures
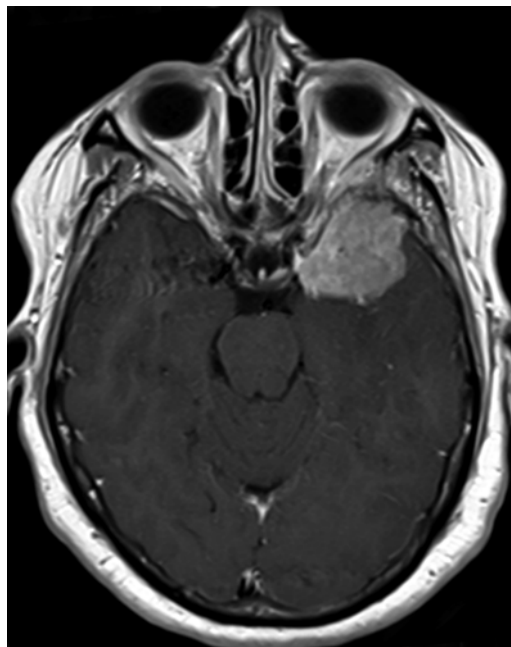
Fig. 9.12 Sphenoid wing meningioma. Axial post-contrast spin echo T1 image demonstrates large homogeneously enhancing meningioma along the greater wing of the left sphenoid with extension to the orbital apex. The tumor exerts moderate mass effect on the adjacent left temporal pole and there is suggestion of associated hypointense white matter signal, indicating reactive edema
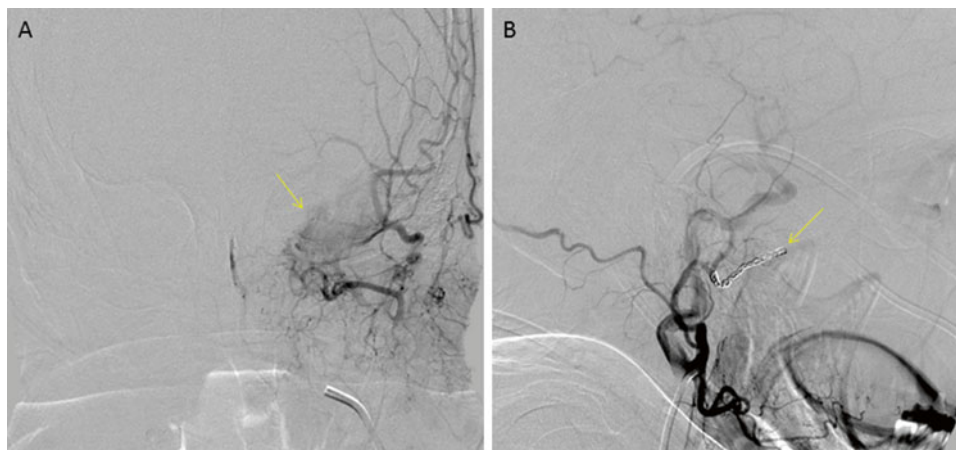
Fig. 9.13 Embolization of the sphenoid wing meningioma in Fig. 9.12. (**A**) Coronal projection DSA image demonstrates tumoral blush along the greater wing of the left sphenoid bone after injection of the left internal maxillary artery. (**B**) Lateral projection demonstrates successful coil embolization of the internal maxillary feeding branch as evidenced by lack of tumoral blush

References

1. Beckmann EC. CT scanning the early days. Br J Radiol. 2006; 79:5–8.
2. Kalender WA, Seissler W, Klotz E, Vock P. Spiral volumetric CT with single-breath hold technique, continuous transport, and continuous scanner rotation. Radiology. 1990;176:181–3.
3. Ding J, Sun G, Lu Y, et al. Evaluation of anterior ethmoidal artery by 320-slice CT angiography with comparison to three-dimensional spin digital subtraction angiography: initial experiences. Korean J Radiol. 2012;13:667–73.
4. Müller-Forell WS. Computed tomograpy. In: Müller-Forell WS, editor. Imaging of orbital and visual pathway pathology. Berlin: Springer; 2002. p. 15–7.
5. Rhee CM, Bhan I, Alexander EK, Brunelli SM. Association between iodinated contrast media exposure and incident hyperthyroidism and hypothyroidism. Arch Intern Med. 2012;172:153–9.
6. Mumtaz M, Lin LS, Hui KC, Mohd Khir AS. Radioiodine I-131 for the therapy of Graves' disease. Malays J Med Sci. 2009;16:25–33.
7. Shah DJ, Sachs RK, Wilson DJ. Radiation-induced cancer: a modern view. Br J Radiol. 2012;85:e1166–73.
8. Tan JS, Tan KL, Lee JC, et al. Comparison of Eye lens dose on neuroimaging protocols between 16- and 64-section multidetector CT: achieving the lowest possible dose. AJNR Am J Neuroradiol. 2009;30:373–7.
9. ICRP. ICRP statement on tissue reactions. International Committee on Radiological Protection. 2011.
10. Silva AC, Lawder HJ, Hara A, et al. Innovations in CT dose reduction strategy: application of the adaptive statistical iterative reconstruction algorithm. AJR Am J Roentgenol. 2010;194:191–9.
11. Bose S, Rubin R. Principles of imaging in neuro-ophthalmology. In: Yanoff M, editor. Ophthalmology. Philadelphia: Mosby/Elsevier; 2009. p. 943–9.
12. Yousem DM, Grossman RI. Orbit. In: Yousem DM, Grossman RI, editors. The requisites. Neuroradiology. Philadelphia: Mosby/Elsevier; 2010. p. 1–20. 321–355.
13. Fanea L, Fagan AJ. Review: magnetic resonance imaging techniques in ophthalmology. Mol Vis. 2012;18:2538–60.
14. Gandhi RA, Nair AG. Role of imaging in the management of neuro-ophthalmic disorders. Indian J Ophthalmol. 2011;59:111–6.
15. Belden CJ, Zinreich SJ. Orbital imaging techniques. Semin Ultrasound CT MR. 1997;18:413–22.
16. Lee AG, Johnson MC, Policeni BA, Smoker WR. Imaging for neuro-ophthalmic and orbital disease—a review. Clin Experiment Ophthalmol. 2009;37:30–53.
17. Quality and Safety- American College of Radiology. www.acr.org/~/media/ACR/Documents/PDF/QualitySafety/Resources/Contrast%20Manual/Contrast%20Nephrotoxicity.pdf
18. Pollok JM, Tan H, Kraft RA, et al. Arterial spin labeled MRI perfusion imaging: clinical applications. Magn Reson Imaging Clin N Am. 2009;17:315–38.
19. Ilica AT, Kocacelebi K, Savas R, Ayan A. Imaging of extranodal lymphoma with PET/CT. Clin Nucl Med. 2011;36:e127–38.
20. Duong TQ, Ngan SC, Ugurbil K, Kim SG. Functional magnetic resonance imaging of the retina. Invest Ophthalmol Vis Sci. 2002;43:1176–81.
21. Herrick RC, Hayman LA, Taber KH, et al. Artifacts and pitfalls in MR imaging of the orbit: a clinical review. Radiographics. 1997; 17:707–24.
22. Obata T, Uemura K, Nonaka H, et al. Optimizing T2-weighted magnetic resonance sequences for surface coil microimaging of the eye with regard to lid, eyeball and head moving artifacts. Magn Reson Imaging. 2006;4:97–100.
23. Duvoisin B, Zanella FE, Sievers KW. Imaging of the normal and pathological orbit. Neuroradiology. 1998;8:175–88.
24. Hasegawa M, Fujisawa H, Hayashi Y, et al. CT arteriography for orbital tumors: diagnostic and surgical value. J Clin Neurosci. 2005;12:548–52.
25. Schumacher M, Schmidt D, Jurklies B, et al. Central retinal artery occlusion: local intra-arterial fibrinolysis versus conservative treatment, a multicenter randomized trial. Ophthalmology. 2010; 117:1367–75.
26. Reese AB, Hyman GA, Merriam GR, et al. Treatment of retinoblastoma by radiation and triethylenemelamine. Am J Ophthalmol. 1954;53:505–13.
27. Gobin YP, Dunkel IJ, Marr BP, et al. Intra-arterial chemotherapy for the management of retinoblastoma: four-year experience. Arch Ophthalmol. 2011;129:732–7.
28. Shields CL, Bianciotto CG, Jabbour P, et al. Intra-arterial chemotherapy for retinoblastoma: report no. 1, control of retinal tumors, subretical seeds, and vitreous seeds. Arch Ophthalmol. 2011;129: 1399–406.
29. Shields CL, Bianciotto CG, Jabbour P, et al. Intra-arterial chemotherapy for retinoblastoma: report no. 2, treatment complications. Arch Ophthalmol. 2011;129:1407–15.